Acoustic properties of plates with unevenly distributed macro perforations backed by woven meshes

Heidi Ruiz, Pedro Cobo, Thomas Dupont, Bruno Martin, Philippe Leclaire

Acoustic properties of plates with unevenly distributed macro perforations backed by woven meshes

Heidi Ruiz[a)] and Pedro Cobo

Center for Applied Acoustics and Non Destructive Testing CAEND,

CSIC-UPM,

Serrano 144,

28006 Madrid,

SPAIN

Thomas Dupont, Bruno Martin, and Philippe Leclaire

Département de Recherche en Ingénierie des Véhicules pour l'Environnement,

ISAT,

Université de Bourgogne,

49 Rue Mademoiselle Bourgeois,

58027 Nevers Cedex,

France

(Dated: February 7, 2012)

Abstract

A hybrid model describing the acoustic properties of plates with macro-perforations that can be unevenly distributed on the plate surface and backed by woven or precision woven meshes with microscopic perforations is proposed. The plate perforations may be of circular or rectangular shapes. Since the perforated plate may not necessarily be considered as an equivalent fluid, its surface impedance is calculated by the Maa model [Noise Control Eng. J. **29**, 77-84 (1987)], whereas the Johnson-Champoux-Allard model [J. Appl. Phys. **70**, 1975-1979 (1991)] is used for the mesh, considered as an equivalent fluid. A simple model for the elementary cell of the mesh structure is proposed in order to calculate a parameter that can be considered as the thermal length. It is shown that, this thermal length can be smaller than the length considered as the viscous length. An effective airflow resistivity is introduced to account for the increase of particle velocity through the mesh placed behind the carrying macroperforated plate and is used in the transfer matrix approach to obtain the impedance of the whole multilayer system. The hybrid model seems to represent a good approach of this multilayer system. The theoretical predictions are compared with experimental measurements.

PACS numbers: 43.55.Ev,43.50.Gf,43.20.Hq

I. INTRODUCTION

The acoustical behavior of perforated panels has been an important research topic over the last decades. The analytical model proposed by Maa[1] is frequently used to predict the acoustic impedance of a microperforated panel (MPP) with circular perforations. The equation for the impedance combines the model of sound propagation in narrow tubes studied by Rayleigh and Crandall[2,3], and includes the end corrections done by Ingard[4]. In the useful audible frequency range, the best performance for perforated panels is obtained for submillimetric holes. As recommended by Maa[1], the diameter of perforation - to - thickness ratio should be close to one to obtain optimal absorption properties. Manufacturing panels with submillimetric holes and submillimetric thicknesses can be a difficult task in practical acoustic engineering applications. Furthermore, drilling a large amount of submillimetric holes in a panel (usually done by laser technology) can be expensive. An alternative method to reduce the amount of perforations while keeping the porosity equal to that of an MPP is to use slits[5,6]. Manufacturing a panel bearing slits (MSP) can be less expensive than an MPP.

A perforated plate can in some cases also be modeled as a rigid frame porous medium described by the well established Johnson-Champoux-Allard (JCA) theory[7–9] that depends on five physical parameters: the thermal Λ' and viscous Λ characteristic lengths, the porosity ϕ, the tortuosity α_∞, and the static air flow resistivity σ. Atalla and Sgard[10] presented an equivalent fluid approach that considers these parameters. The analytical models of Maa and the equivalent fluid approach agree in what concerns the impedance inside the perforations. Nevertheless, the end corrections differ. While Maa[1,5] introduces the end correction as an additional complex impedance with resistive and reactive components, Atalla and Sgard[10] introduce the end correction by means of the geometric tortuosity α_∞ as a multiplying factor of the effective density $\tilde{\rho}_e$.

To increase the sound attenuation, perforated panels can be backed by porous materials or textiles[11–13]. Combining a carrying plate with a commercial woven mesh makes it possible to design an absorber with a performance similar to that of a single-layer MPP. Indeed, Pfretzschner *et*

[a)]Electronic address: heidi@caend.upm-csic.es

al.[12] proposed a design procedure that consisted on combining a perforated panel and a micrometric mesh with appropriate constitutive parameters, which they named a microperforated insertion unit (MIU). The impedance of the MIU combination resulted from the addition of the acoustic impedances of the perforated plate and of the wire mesh divided by the open area fraction of the plate ϕ. The impedance of the system was then obtained by the impedance transfer method[14].

Recently, Chevillote[13] studied the role of a resistive layer upstream on a porous medium. The resistive layer, was then modeled using the JCA equivalent fluid model[7–9]. The acoustic impedance of such resistive layer was obtained using the transfer matrix method[7]. Chevillote used a 2D microscopic characterization with help of a picture processing to determine the hydraulic radius and deduce the thermal characteristic length of the textile.

In this article, we study a multilayer system made of macroperforated metal plates backed by microperforated woven textile meshes. This solution involving fairly high perforation radii for the carrying plate and widely available textiles can significantly decrease the costs of manufacturing of the acoustic system. The prefixes ”micro” or ”macro” are related to the relative importance of the radius with respect to the viscous skin depth inside the perforation.

In the present study, a new approach involving a simple model for the elementary cell of the woven textile structure is proposed to estimate more precisely the thermal characteristic length. Also, a hybrid model capable of describing non-homogenously distributed macroperforated panels backed by woven textiles is proposed. The carrying plate is modeled using the analytical approach[1,5] of Maa whereas the JCA model is used in the rigid frame approximation for the mesh. The hybrid model is valid for carrying panels with circular or slit-like macroperforations regardless of their distribution over the surface. Another original aspect developed in this article is the introduction of an effective resistivity. The flow resistivity of the mesh is calculated by means of the shape factor described by Stinson and Champoux[15]. In addition, whereas in Ref. 12 the fact that bonding the membrane to the carrying plate modified the perforation rate of the screen, it is shown in the present study that the modification can be accounted for through the use of an effective resistivity.

The description of the theory used to obtain the impedance of the carrying plate is presented in

section II. The calculation of the thermal characteristic length of microperforated woven meshes is described in section III. Section IV presents the hybrid model using a combination of the models of Maa and JCA in the context of the transfer matrix method and also the derivation of the effective flow-resistivity. Experimental validation is presented in the last section.

II. PERFORATED PLATE

The surface impedance of a perforated panel can be written as the sum of two contributions[1,5]: the impedance at the interior of the perforation and the impedance at the borders which accounts for the end corrections:

$$Z_1 = \frac{\sqrt{2}\mu y}{\phi d} + \frac{j\omega\rho_0}{\phi}\Big[R\psi(\xi)r + \frac{t}{[1+S]}\Big], \tag{1}$$

where μ is the air kinematic viscosity coefficient, ρ_0 the air density, ω the angular frequency, t the panel thickness, r the perforation radius, ϕ the perforation ratio, and $y = d/\sqrt{4\mu/\rho\omega}$ with d the perforation diameter. R and S are parameters that depend on the geometry of the perforations, in particular on the length of the slit l. In the case of periodic hole arrangement, $\psi(\xi)$ is a correction of the reactance term of the end correction that takes into account the interaction between holes when the perforation ratio is high[16,17].

The end corrections studied by Rayleigh and Ingard[2,4] are included in the first and second term of Eq. (1). The influence of a mass of air contained in a cylindrical volume for which the apparent length is greater than the plate thickness is included in the numerator of the second term. The third term represents the impedance of the perforations which has been studied by Crandall[3] for an array of tubes and by Ingard[4] for an elliptic aperture. The velocity profile of the flow through the holes is determined by the term y. The values of R, S and $\Psi(\xi)$ are shown in Table I where J_0, J_1 are Bessel functions of the first kind and order 0 and 1, respectively and $F_{(e)}$ is an elliptic integral with $e = \sqrt{1-(r/l)^2}$.

$$F_{(e)} = \frac{\pi}{2}\left[1 + \left(\frac{1}{2}\right)^2 e^2 + \left(\frac{1\times 3}{2\times 4}\right)^2 e^4 + \left(\frac{1\times 3\times 5}{2\times 4\times 6}\right)^2 e^6 + ...\right], \tag{2}$$

The equation of impedance described by Randeberg in Ref. 6, includes the interaction between perforations as well as the resistive and reactance end corrections deduced for the modified depth

of the slit[18]. For the present study, the equations proposed by Maa will be used to model a macro-perforated carrying plate.

III. MICROMETRIC MESH

The absorption of textiles and microperforated membranes has been calculated by Kang and Fuchs using the equation of impedance given by Maa. In a recent study, Atalla and Sgard considered a plate or screen as an equivalent fluid using the rigid frame porous model developed by Johnson-Champoux-Allard[7–9]. The model by Maa and that of Atalla and Sgard are similar in what concerns the impedance inside the perforations. However, in the equivalent fluid approach, the end corrections are introduced by means of the tortuosity allowing to define the boundary conditions in multilayer configurations. Latest works apply this model for woven or non-woven fabrics[13,19]. In many cases, a homogeneous cross section of perforations is considered (for example cylindrical or square cross section). Nevertheless, as the woven meshes studied here exhibit more complex squared pore geometries, a more specific approach is needed (three dimensions approach is required for some parameter characterizations).

In the JCA model, the tortuosity, resistivity, porosity and characteristic lengths of the pores can be obtained[8] or measured for each specific equivalent fluid. The visco-thermal effects associated with a wave impinging onto a porous medium can be modeled introducing a complex dynamic density i.e, the effective density $\rho_e(\omega)$ (see ref. 7).

$$\tilde{\rho}_e(\omega) = \alpha_\infty \rho_0 \left(1 + \frac{\sigma\phi}{j\omega\rho_0\alpha_\infty} \sqrt{1 + \frac{j\omega 4\alpha_\infty^2 \mu\rho_0}{\sigma^2\Lambda^2\phi^2}} \right), \tag{3}$$

where α_∞ is the tortuosity, ρ_0 the air density, σ the flow resistivity, ϕ the porosity, which is considered equivalent to the perforation ratio, ω the angular frequency, μ is the air kinematic viscosity coefficient and Λ is the viscous length given by[8]

$$\frac{2}{\Lambda} = \frac{\int_s v_i^2(r_w) dS}{\int_v v_i^2(r) dV}. \tag{4}$$

The integrations of the numerator and the denominator of Eq.(4) are over the walls of the pore perforation and over the pore volume respectively.

Equation (3) indicates that the parameters α_∞ and σ are important factors in the calculation of the effective density. While the flow resistivity depends on the pore shape, the tortuosity depends on the pore shape and the layer arrangement. For a screen with air at both sides, $\alpha_\infty = 1 + (2\varepsilon/t)$ where ε represents a correction length.

The classical MPP's formulation[20] and the equivalent fluid MPP's approach[10] take into account the increase of kinetic energy caused by the sound radiation effect at the end openings of perforations and the distortion effect of the acoustic flow at the panel surface. As a result, the MPP's reactance must be supplemented by an additional mass by way of the length correction ε on the plate thickness, in the imaginary part of the MPP's impedance[4,7]. In the case of a single perforation, the classical approach employs an analogy with the radiation impedance of a rigid piston with a circular cross section flanged in an infinite rigid wall. For this approach the end termination of perforation is considered to have a sharp edge. In the present study, however, the end termination of the screen perforation has rounded edges. This kind of edge tends to diminish the length correction[21]. Moreover, when there are several perforations in close proximity, one must consider that the interaction between perforations tends to diminish the length correction[4,6]. For the meshes treated in this study, the flange between two perforations is small compared to their size, which causes a strong interaction between the rounded edges of the pore. The length correction is thought to be very small and is therefore disregarded. As a result, the effective tortuosity is equal to 1.

The flow resistivity σ has been described by Stinson and Champoux[15] for simple pore shapes as

$$\alpha = \frac{4k_0\mu\alpha_\infty^2}{h_r^2\phi}, \tag{5}$$

where, h_r is the hydraulic radius and k_0 is a constant parameter for a given pore shape. When the perforations are assumed of cylindrical shape with constant cross section, the viscous characteristic length and the thermal characteristic length are equal to the hydraulic radius of the perforation[7,10,13,19] $\Lambda{=}\Lambda'{=}h_r{=}d/2$. However as will be seen in the next section, this assumption cannot be made for other pore geometries.

Considering woven membranes as materials with identical uniform pores, the effective density

can be linked to the dynamic bulk modulus given by[7,9]

$$K(\omega) = \frac{\gamma P_0}{\gamma - (\gamma - 1)(1 + H\sqrt{1 + j\omega/H}/2j\omega)}, \tag{6}$$

where γ is the fluid specific heat ratio, P_0 is the fluid equilibrium pressure, ω the angular frequency and $H = 16\mu/(N_{Pr}\Lambda^{'2}\rho_0)$. N_{Pr} is the Prandtl number. The thermal length $\Lambda^{'}$ characterizes the high frequency behavior of the bulk modulus[9]. A simple model to calculate Λ' is presented in section III.A.

Equations (3) and (6) allow to calculate the characteristic impedance Zc of the fluid,

$$Z_c = \sqrt{K(\omega)/\tilde{\rho_e}(\omega)}, \tag{7}$$

and the associated wave number

$$k = \omega\sqrt{\tilde{\rho_e}(\omega)/K(\omega)}. \tag{8}$$

A. Simple model for calculating the thermal length of woven meshes

The thermal characteristic length has been defined as the surface to pore volume ration of the pore solid interface[9]

$$\frac{2}{\Lambda'} = \frac{\int_S dS}{\int_V dV} = \frac{S}{V}. \tag{9}$$

The volume of air passing through the pore depends on the end termination of the yarn geometry. Assuming isotropic meshes with cylindrical yarns, an original model to obtain the thermal length is proposed. The elementary cell of the screen perforation is shown in Figure 1.

A simple calculation can be made by observing a single perforation as the one in Figure 2a. The volume of air through the cell is observed in Figure 2b.

The volume of each truncated cylinder in the elementary cell of Figure 2a is

$$V_h = \pi r_y^2 b - 4\int_{-r_y}^{ry}\int_0^{\sqrt{r_y^2 - x^2}} y dx dy, \tag{10}$$

where r_y is the yarn radius and $b = d + 2r_y$. Solving the integral of the second term in the right hand side of Eq.(10) gives

$$V_h = \pi r_y^2 b - 4\frac{2r_y^3}{3}. \tag{11}$$

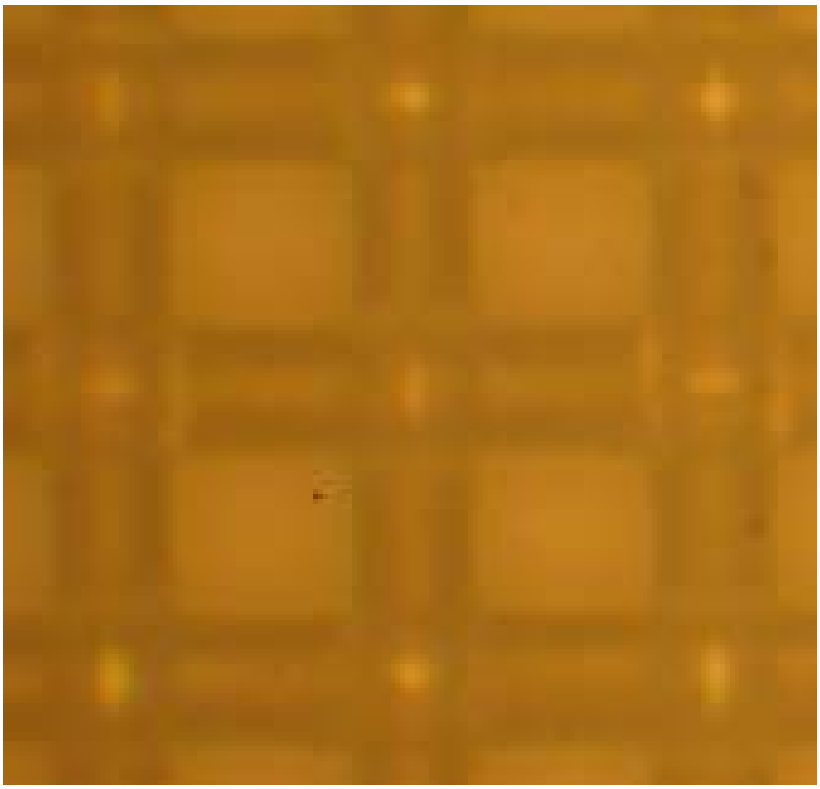

FIG. 1. (color online)Microscopic image of an elementary cell of a woven mesh.

The volume V_p of the pore (Figure 2b) is then

$$V_p = b^2 Y_d - \frac{4V_h}{2}. \tag{12}$$

Figure 2b represents Eq.(12). The surface of each truncated cylinder is

$$S_h = 2\pi r_y b - 4\int_0^{\pi} r_y^2 sin\theta d\theta. \tag{13}$$

Solving the integral in Eq.(13) we obtain

$$S_h = 2\pi r_y b - 8r_y^2. \tag{14}$$

The interior surface S_p of the pore is then

$$S_p = \frac{4S_h}{2}. \tag{15}$$

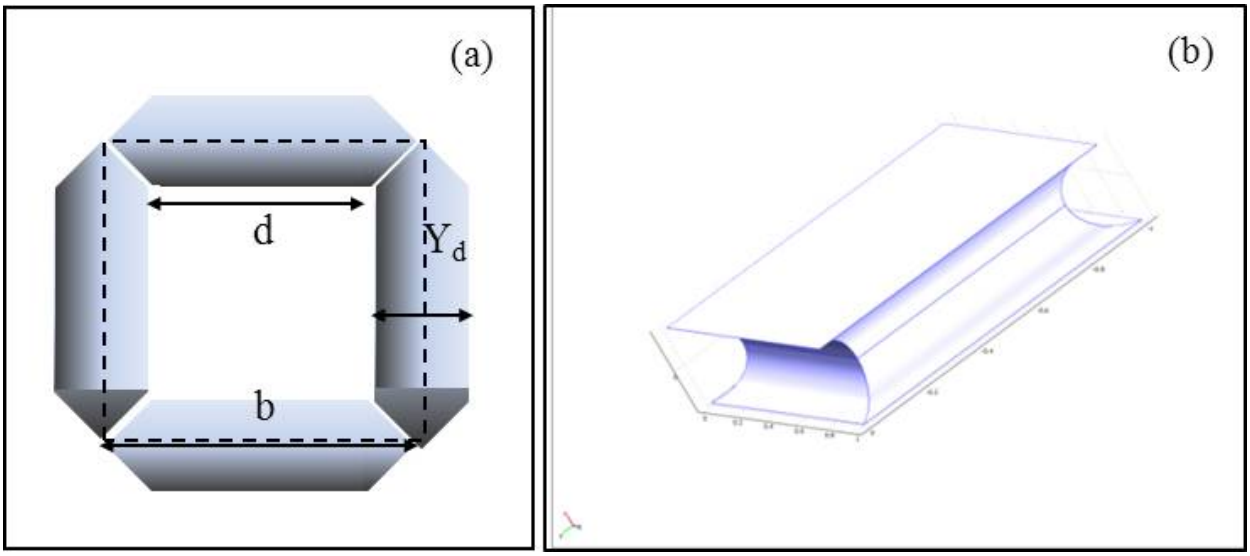

FIG. 2. (color online)Simple model for a single mesh perforation geometry. a) fiber structure (the dotted rectangle represents the elementary cell), b) inside volume.

The thermal length can be obtained replacing S_p in S and V_p in V in Eq.(9).

$$\Lambda' = \frac{b^2 - b\pi r_y + (8/3)r_y^2}{\pi b - 4r_y}. \tag{16}$$

In the examples studied, it is found that the thermal characteristic length calculated via Eq.(16) can be smaller than the viscous characteristic length. This result tends to show that for the microstructure studied, the thermal effect can have a large influence on the bulk modulus at high frequencies. Assuming identical pores for the particular geometry of a square pore of woven meshes, the physical parameters are: $\Lambda = r$, $\alpha_\infty = 1$, σ is obtained with Eq.(5) where[15] $k_0 = 1.78$, Λ' is obtained with Eq.(16) and $\phi = (d/(Y_d + d))^2$.

IV. THE HYBRID MODEL AND THE TRANSFER MATRIX APPROACH.

In the work of Pfretzschner et al., the impedance of a system composed of a perforated plate carrying a micrometric mesh was obtained using the impedance transfer method[12,14]. Kang and Fuchs[11] used the electrical circuit approach for the same purpose. In the present work, the transfer matrix approach[7] is used and the acoustic impedance of the whole system is obtained considering the impedance matrix of each element.A hybrid model combining the Maa and the JCA model to

obtain the input impedance of a system composed of a macro-perforated plate and a micrometric commercial woven mesh is proposed.

The absorption curve of the hybrid model Maa-JCA depends on 7 parameters $(d_1, t_1, \phi_1, d_2, t_2, \phi_2, D)$, where $d_1, t_1, \phi_1, d_2, t_2, \phi_2$ are the pore diameter, thickness and porosity of the carrying plate and the mesh respectively, and D is the air cavity thickness. Using Eq.(1), the impedance matrix for a carrying plate with circular or slits perforations can be obtained as

$$T_{plate} = \begin{bmatrix} 1 & j(imag(Z_1)) \\ 0 & 1 \end{bmatrix}. \tag{17}$$

In this study, carrying plates with perforations sizes greater than 1 mm and perforations rates close to 10% are considered, the viscous characteristic frequency is very low, so the thermo-viscous effect can be disregarded[7]; however, the mass effect is very high. As a consequence the impedance expression could be reduced in such a way that only the imaginary part is taken into account. Indeed, the experimental sound absorption coefficient of this plate (MPP or MSP without screen) coupled with an air cavity and rigid wall is weak.

The matrix for a mesh in the equivalent fluid context is given by

$$T_{Mesh} = \begin{bmatrix} cos(k_M t_M) & jZ_{cM} sin(k_M t_M)/\phi_M \\ \phi_M Z_{cM} sin(k_M t_M) & cos(k_M t_M) \end{bmatrix}, \tag{18}$$

where t_M,ϕ_M,Z_{cM},k_M are the thickness, the porosity, the characteristic impedance and the wave number of the fluid in the mesh, respectively Z_{cM},k_M can be obtained with Eq.(7) and (8) respectively.

For the air cavity, t_M,ϕ_M,Z_{cM},k_M are replaced by the properties of air i.e. D, 1, Z_{cA}, k_A which represent the thickness, the porosity, the characteristic impedance and wave number of the air in the cavity. The corresponding matrix is

$$T_{Air} = \begin{bmatrix} cos(k_A t_A) & jZ_{cA} sin(k_A t_A)/\phi_A \\ \phi_A Z_{cA} sin(k_A t_A) & cos(k_A t_A) \end{bmatrix}. \tag{19}$$

A transfer matrix can be adapted for each new layer of plate, mesh or air. The multilayer configuration is obtained with Eq.(24).

The schematic represented in Figure 3 shows the effect of the flow inside the perforations. The particle velocity is the same at both sides of the hybrid system. As ϕ_1 and ϕ_2 are always smaller than 1, the particle velocity inside the pores is always greater than outside them. The relationship between the pressure gradient ΔP and the particle velocity is described by Darcy's law as:

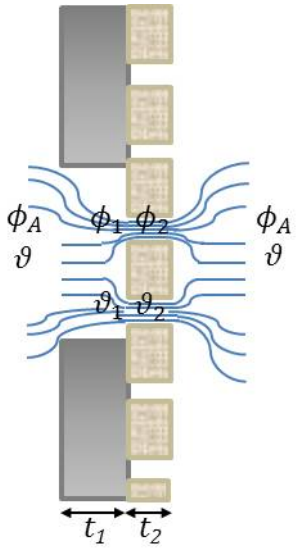

FIG. 3. (color online)Viscous flow of the fluid through the perforations. Downstream the perforation, the "apparent" fluid velocity in the mesh is increased because of the squeezing due to the presence of the perforations upstream. This results in an "effective flow resistivity" that accounts for this diaphragm effect.

$$\Delta_P = -\phi\vartheta\sigma. \tag{20}$$

This equation can be used to describe the flow in the woven mesh. However, when a macroperforated plate is coupled with a mesh without airspace between the two elements, a correction should be applied to this law to incorporate a "diaphragm effect" (Fig. 3). As the flow is squeezed inside the plate macroperforations, the flow velocity at the entrance of the pores of the mesh is increased and the flow resistivity of the mesh should be modified to account for this phenomenon. The correction factor on the flow resistivity is precisely the porosity of the carrying plate. As a result, the resistivity of the mesh should be replaced by an "effective resistivity" of the combination

plate-mesh

$$\sigma_{eff} = \frac{\sigma_{mesh}}{\sigma_{plate}}. \tag{21}$$

Therefore the modified Darcy law for the mesh is

$$\Delta P = -\phi_{mesh}\vartheta_{mesh}\frac{\sigma_{mesh}}{\sigma_{plate}}, \tag{22}$$

and

$$\Delta P = -\phi_{mesh}\vartheta_{mesh}\sigma_{eff}. \tag{23}$$

The multiplication of the individual matrices results in the global transfer matrix of the hybrid model:

$$T_h = [T_{Plate}][T_{Mesh}][T_{Air}]. \tag{24}$$

The input impedance of the system and absorption coefficient are then obtained by

$$Z_h = \frac{T_{11}^h}{T_{21}^h}, \tag{25}$$

$$\alpha = 1 - \left|\frac{Z_h - Z_0}{Z_h + Z_0}\right|^2. \tag{26}$$

The effect of modifying the mesh resistivity by the effective resistivity is shown in Figure 4.

V. EXPERIMENTAL RESULTS

The experiments were carried out in a laboratory where the atmospheric conditions were: T=23°C, P_o = 103070 Pa, c = 344.9 m/s, ρ_0 = 1.21 kg/m^3, $\mu = 1.83 \times 10^{-5}$ Kg $m^{-1}s^{-1}$, γ = 1.4 and N_{pr} = 0.71. Figure 5 shows the absorption curve of a commercial woven mesh placed in front of a rigid wall (d, t, ϕ, Y_d, D)=(36 μm,50 μm,28 %,33 μm,5 cm), where d is the diameter of perforations, t the thickness, ϕ the perforation ratio, Y_d the yarn diameter and D the air cavity thickness. A good agreement between the JCA model and the measurement is achieved. For this example, the manufacturer's nominal parameters where used and good results were obtained. The real and imaginary parts of the dynamic tortuosity and bulk modulus of air in the mesh are observed in Figure 6. The experimental validation of the hybrid model is now proposed. Figure

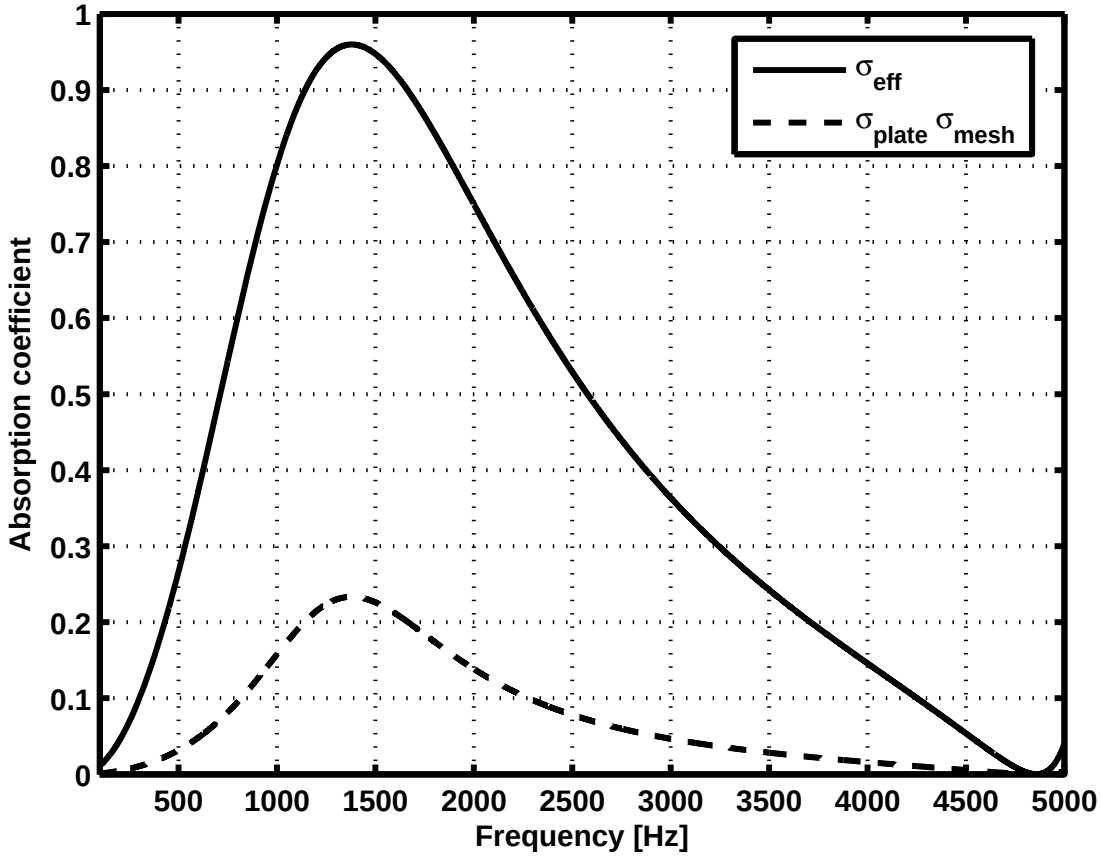

FIG. 4. Absorption curve of a carrying plate with (d_1, t_1, ϕ_1) = (3 mm, 1 mm, 10 %) with a micrometric mesh (d_2, t_2, ϕ_2)=(50 μm, 50 μm, 37 %) and D=3.5 cm. $(-)$ with correction for resistivity, $(--)$ without correction.

7 shows the four different macro-perforated carrying plates with d=3, ϕ = 9.96 % and t=1 mm. In plates 1, 2 and 4 the hydraulic diameter is equal to $r_h = \Lambda' = ld/(l + d)$, while in plate 3 $r_h = \Lambda = d/2$. A good adjustment is obtained for ξ = 0.25, 0.25, 0.35 and 0.28 for plates 1 to 4 respectively. Precision woven (meshes b, c and e) and non-precision woven (a and d) meshes where tested.

Figure 8 shows the five meshes used. The pores and yarn diameter were obtained using the software Optika vision lite and an Euromex Holland microscope. The microscopic analysis allowed to calculate the thermal and viscous characteristic lengths. The thickness was measured

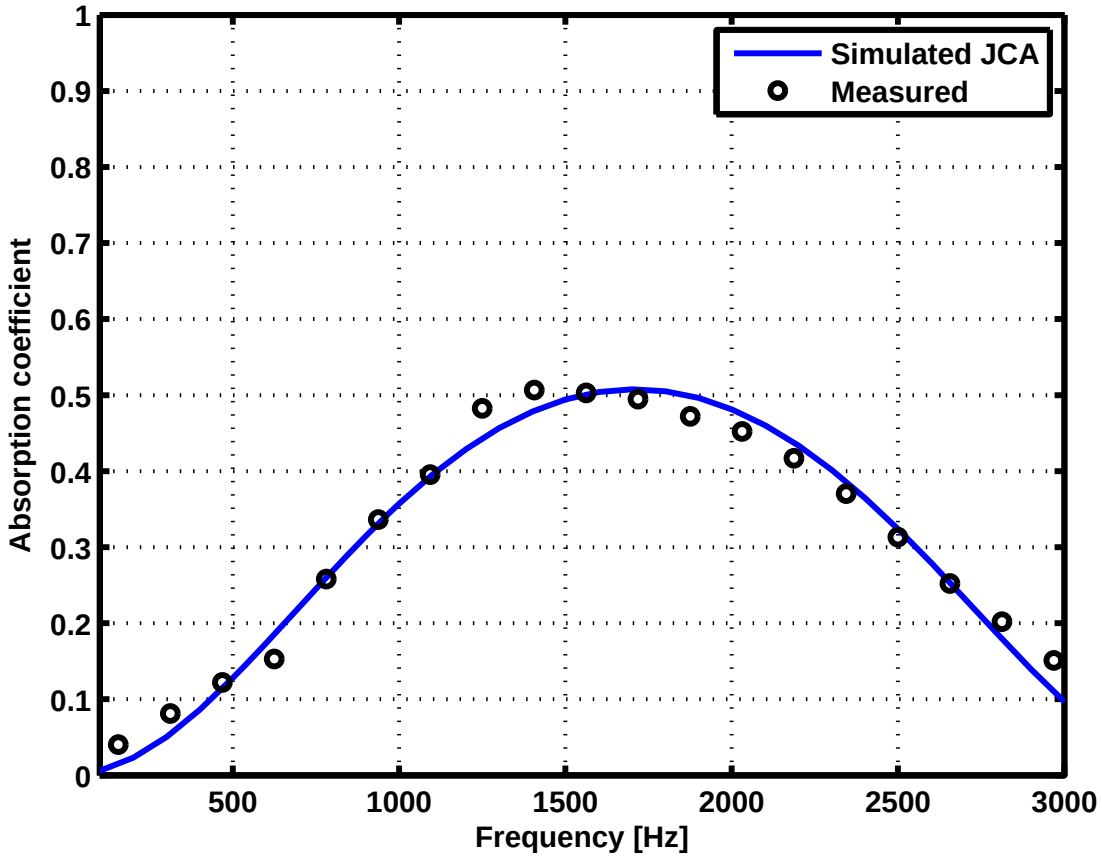

FIG. 5. (color online)Absorption curve of a mesh with parameters (d, t, ϕ, Y_d, D)=(36 μm,50 μm,28 %,33 μm,5 cm)

with a digital caliper. The porosity was also evaluated by the expression $\phi = (d/(Y_d + d))^2$. The precision on the evaluation of the porosity when compared to the manufacturer's value was 5%. Results are shown in Table 2. It is seen that when $Y_d \geq 3.3d$, the thermal length calculated by Eq. (16) is smaller than the viscous length taken to be equal to half the interfiber distance d. This is the case for all the meshes studied except for mesh a.

Figure 9 illustrates the results of combining plate 1 with meshes a, b and d. Two interesting results are highlighted. First, the hybrid model presents a very good agreement with the experimental measurements for precision woven and non-precision woven meshes. Second, a very high absorption is achieved by using mesh b and d and while the first one is a commercial precision

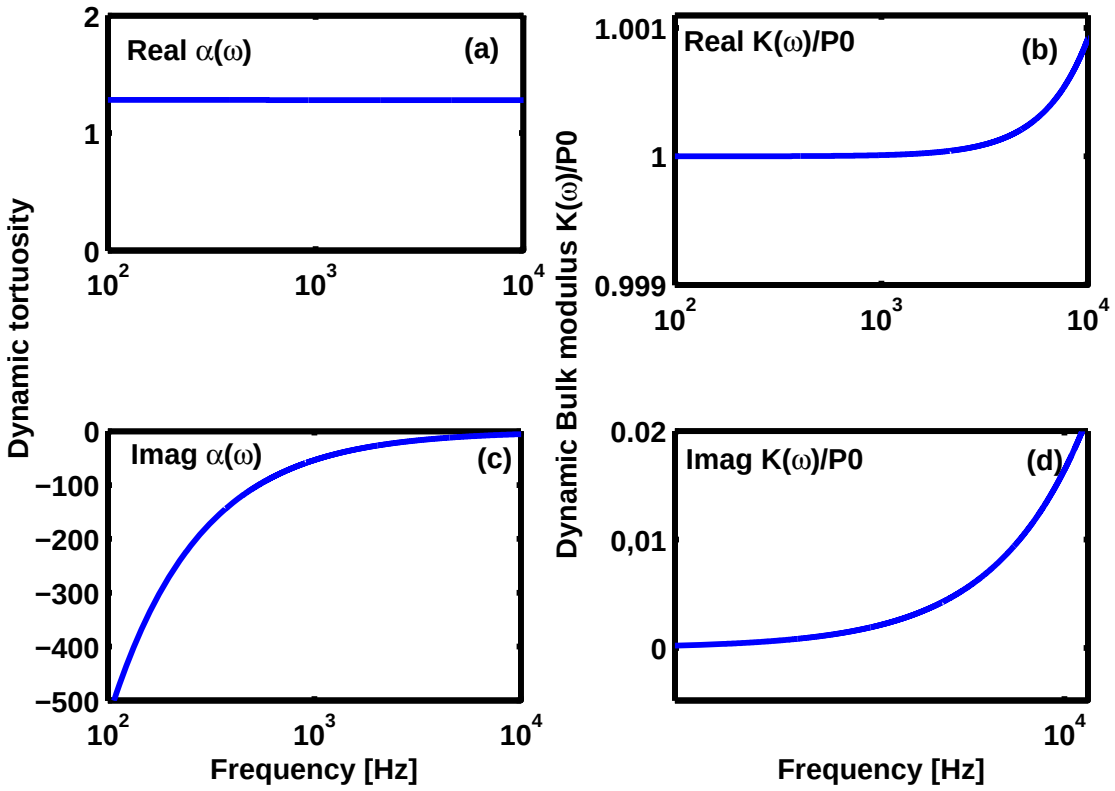

FIG. 6. (color online)Dynamic tortuosity and bulk modulus of air for a precision woven micrometric mesh Sefar Nitex 36/28. a) and b) real parts, c) and d) imaginary parts.

woven mesh used for filtering, the second one is a simple woven curtain. The difference in costs between the two meshes is about 10 times and the results are very similar.

Figure 10 seems to validate the model also for a carrying plate with circular perforations. Mesh *e* is then combined with plates 2 and 4 (P2-HF and P4-HF, see Figure 11). It appears that using the same mesh with two different plates with the same perforation ratio but different perforations distribution provides very similar absorption curve. Deviations from the two curves in Figure 11 are due to the fact that the attached mass in plate 2 is slightly bigger than in plate 4.

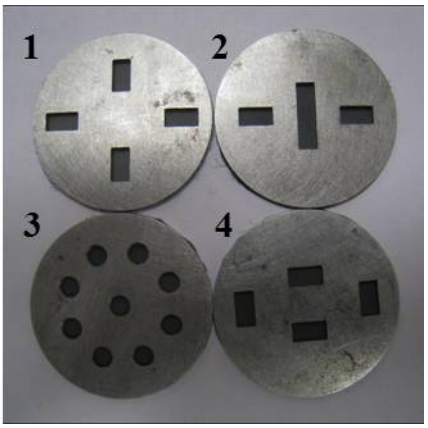

FIG. 7. (color online)MPPs and MSPs with different perforations distribution.

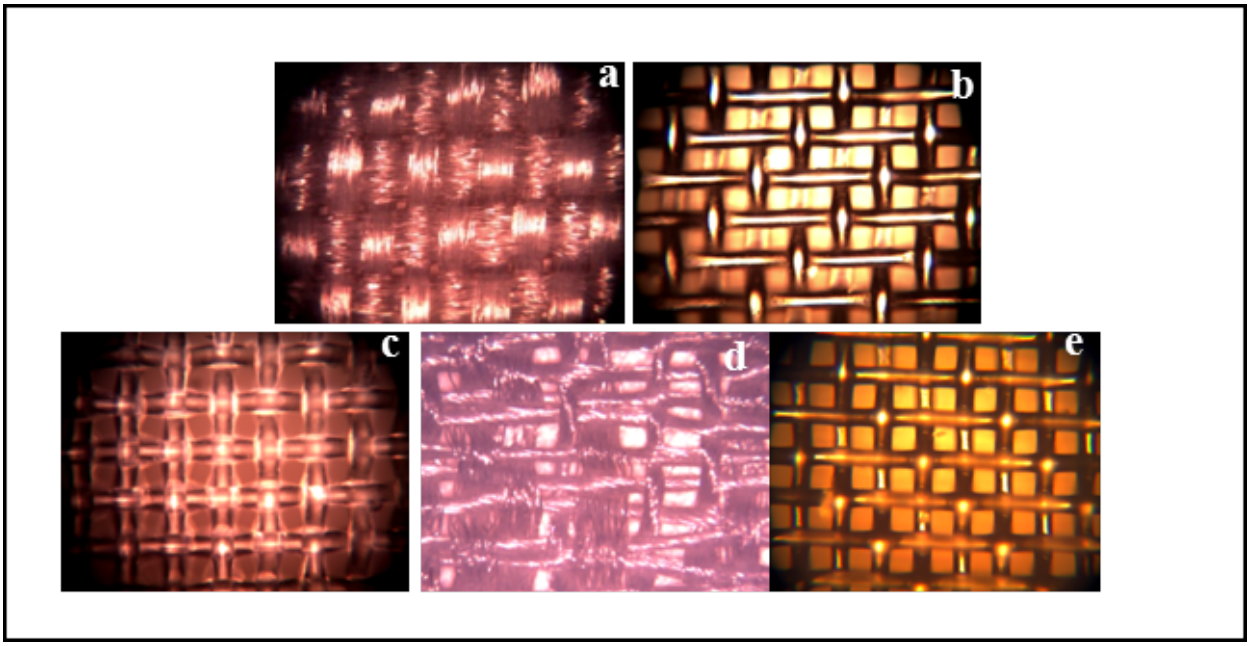

FIG. 8. (color online)Microscopic image of the meshes tested a)Woven screen, b) sefar®acoustic BHY, c) sefar®Nitex 41/31, d) curtain e) sefar acoustic HF 34-39.

VI. CONCLUSIONS

A hybrid acoustic model using a macro perforated carrying plate and a micrometric woven mesh has been proposed. The absorption curve of such system depends on 7 parameters: the constitutive parameters of the panel, the thickness of the air cavity and the parameters of the

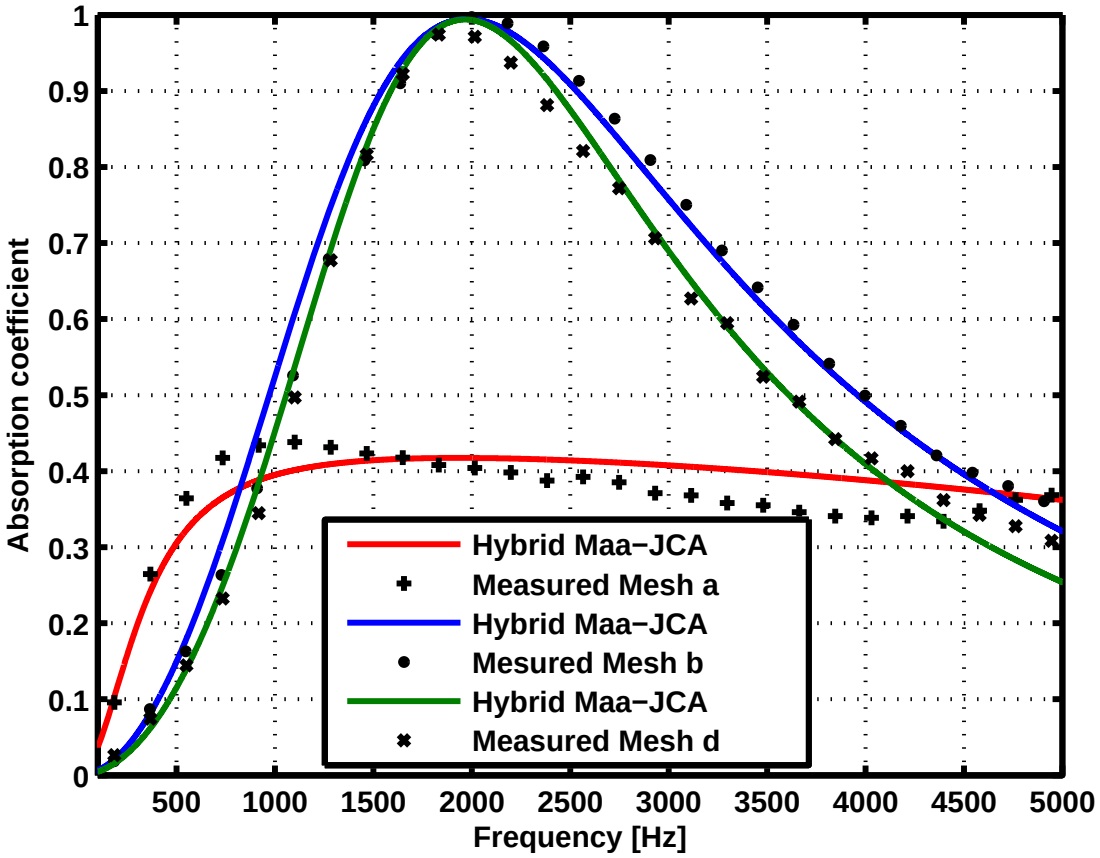

FIG. 9. (color online)Absorption curve of plate 1 combined with mesh a (+), b (o), and d (x). Air cavity D=2 cm.

micrometric mesh.

A simple equation for the calculation of the thermal characteristic length with square pores was used. This equation resulted from a simple modeling of the woven mesh elementary cell. It is found that in the woven mesh geometries studied, the thermal characteristic length can be smaller than the viscous characteristic length. This result tends to show that the thermal effects have a great importance in woven meshes at high frequencies.

A correction of the air flow resistivity of the mesh when placed behind a carrying plate was proposed. This correction accounts for a “diaphragm effect” due to the squeezing of the air flow inside the macroperforation, which results in an effective flow resistivity for the mesh.

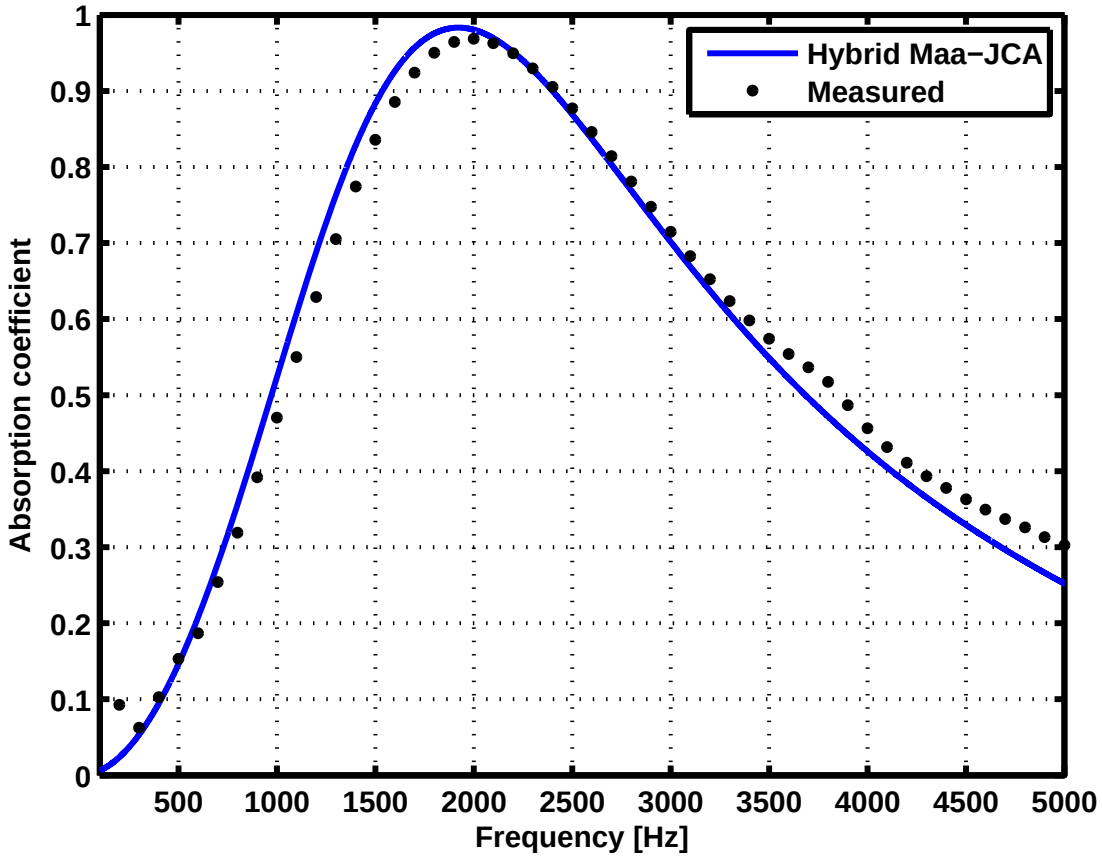

FIG. 10. (color online)Absorption curve of plate 3 combined with mesh *c*. Air cavity D=2.4 cm.

The transfer matrix method allows to handle multilayer configurations. The macroperforated plate can be studied in the framework of the classical Maa model while the porous layer can be modeled as an equivalent fluid with the JCA approach.

The costs of an absorbing system can be considerably reduced by using macro perforated panels and commercial meshes. Panels with perforations of the millimetric order are more manageable and can be drilled easily or even purchased. Micrometric meshes used for filtering are commercially manufactured and even woven curtains can be used for this purpose.

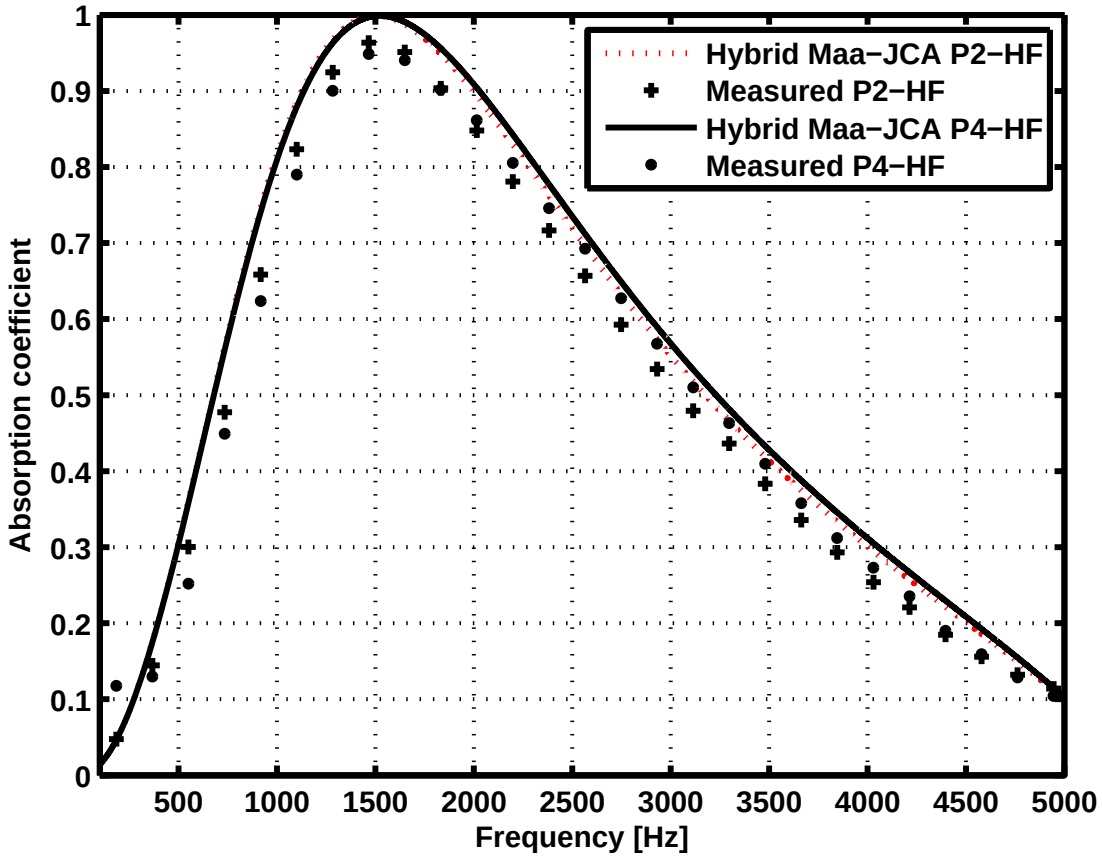

FIG. 11. (color online)Absorption curve of plate 2(+) and plate 4(o) combined with mesh *e*. Air cavity D=3.13 cm.

ACKNOWLEDGMENTS

This work has been supported by the Spanish Ministry of Science and Innovation (MICINN) through Projects TRA2008-05654-C03-03 and TRA2011-26261-C04-01.

References

[1] D.Y. Maa, "Microperforated-panel wideband absorbers", Noise Control Eng. J. **29(3)**, 77-84 (1987).

[2] J.W.S. RayLeigh, *The Theory of sound* (Dover, New York, 1945),pp.319.

[3] J. B. Crandall, *Theory of vibrating systems and sound* (Van Nostrand, New York, 1926), Appendix A.

[4] U. Ingard, "On the theory and design on acoustic resonators", J. Acoust. Soc. Am., **25(6)**, 1037-1061 (1953).

[5] D. Y. Maa, "Theory of microslit absorbers(in Chinese)", Acta Acustica., **25**, 481-485 (2000).

[6] R.T. Randeberg, Perforated panel absorbers with viscous energy dissipation enhanced by orifice design, PhD Thesis, Norwegian University of Science and Technology, Trondheim, (2000).

[7] J.F Allard and N. Atalla, *Propagation of Sound in Porous Media. Modelling Sound Absorbing Materials* (Wiley, Chichester, United Kingdom, 2009), Chap. 5, Chap. 11.

[8] D.L. Johnson, J. Koplik and R. Dashen, "Theory of dynamic permeability and tortuosity in fluid-saturated porous media", J. Fluid Mech. **176**, 379-402 (1987).

[9] Y. Champoux and J.F. Allard, "Dynamic tortuosity and bulk modulus in air-saturated porous media", J. Appl. Phys. **70(4)**, 1975-1979 (1991).

[10] N. Atalla and F. Sgard, "Modeling of perforated plates and screens using rigid frame porous models", J. Sound Vib. **303**, 195-208 (2007).

[11] J. Kang and H.V. Fuchs, "Predicting the absorption of open weave textiles and micro-perforated membranes backed by an air space", J. Sound Vib. **220(5)**, 905-920 (1999).

[12] J. Pfretzschner P. Cobo F. Simon M. Cuesta and A. Fernández, "Microperforated Insertion Units: An alternative strategy to design microperforated panels", Appl. Acoust. **67**, 62-73 (2006).

[13] F. Chevillote, "Controlling sound absorption by an upstream resistive layer", Appl. Acous. **73**, 56-60 (2012).

[14] P. Cobo M. Cuesta and M. Siguero, "Comparison of models describing double layer microperforated absorbers", Noise Control Eng. J. **57**, 10-15 (2009).

[15] M.R. Stinson and Y. Champoux, "Propagation of sound and the assignment of shape factores in model porous materials having simple pore geometries", J. Acoust. Soc. Am. **91(2)**, 685-695 (1992).

[16] T.H. Melling, "The acoustic impedance of perforates at medium and high sound pressure lev-

els", J. Sound Vib. **29 (1)**, 1-65 (1973).

[17] R. Tayong T. Dupont and P. Leclaire, "Experimental investigation of holes interaction effect on the sound absoprtion coefficient of micro-perforated panels under high and medium sound levels", App. Acous. **72**, 777-784 (2011).

[18] H. Ruiz and P. Cobo, *Proposal of alternative designs for microperforated panels*, Proceedings of the 40th International Congress and Exposition on Noise Control Engineering, Internoise. Osaka, Japon. September 4-7, 2011.

[19] L. Jaouen and F.X. B*é*cot, "Acoustical characterization of perforated facings", J. Acoust. Soc. Am. **129(3)**, 1400-1406 (2011).

[20] D.Y. Maa, "Theory and design of microperforated panel sound absorbing constructions", Scientia Sinica, **18**, 55-71 (1975).

[21] J. P. Dalmont C.J. Neverveen and N. Joly, "Radiation of tubes with different flanges: numerical and experimental investigations", J. Sound Vib. **244(3)**, 505-534 (2001).

TABLE I. Values of R, S and $\psi(\xi)$ for different carrying plates.

Type of perforation	R	S	$\psi(\xi)$ with ξ=0.88 d/b
Circular	1.7	$\frac{2}{y\sqrt{-j}}\frac{J_1\sqrt{-j}}{J_0\sqrt{-j}}$	1-1.4092(ξ)+0.33818(ξ)^3+0.06793(ξ)^5
Slit	$F_{(e)}$	$\frac{\tanh(y\sqrt{j}}{y\sqrt{j}}$	-0.02287(ξ)^6+0.03015(ξ)^7-0.01641(ξ)^8

TABLE II. Characteristics of the meshes

Mesh	d (μm)	t (μm)	ϕ (%)	Y_d (μm)	Λ (μm)	Λ' (μm)	σ (Nsm^{-4})	σ_{eff} (Nsm^{-4})
a	59.18	110	5.29	198.21	29.59	29.84	2.82×10^6	2.83×10^7
b	39	49	34.9	33	19.50	13.59	9.84×10^5	9.88×10^6
c	45.7	45.87	36.35	30.1	22.85	15.59	6.85×10^5	6.92×10^6
d	94.25	120	19.7	117.8	47.12	34.78	2.97×10^5	2.99×10^6
e	39	45.37	34.90	30.29	19.50	13.46	$9.84 \times 10^5$4	9.88×10^6

List of Figures